Deliverable 2.3 Analysis of climate change and sea level rise including downscaling of climate scenarios

Work Package 2

Acknowledgement

The research leading to these results has received funding from the European Union Seventh Framework Programme (FP7/2007-2013) under Grant agreement n° 603663 for the research project PEARL (Preparing for Extreme And Rare events in coastaL regions).

pearl
Preparing for Extreme And Rare events in coastaL regions

Authors: MPG, CAM, ICL

Contributing Authors: TUHH

Dissemination level:
PP = Restricted to other program participants (including the Commission Services).

Document Information

Project Number	***603663***	Acronym	**PEARL**
Full Title	Preparing for Extreme and Rare events in coastaL regions		
Project URL	http://www.pearl-fp7.eu/		
Document URL			
EU Project Officer	Eleni Manoli		

Deliverable	Number	D2.3	Title	Analysis of climate change and sea level rise including downscaling of climate scenarios
Work Package	Number	WP2	Title	
Lead Author(s)	Elizalde, Alberto; Mikolajewicz, Uwe.			
Contributing Author(s)	Savre, Julien; Herzog, Michael; Dreier, Norman; Peter Froehle; Pain, Christopher; Fang, Fangxin			

Date of Delivery	Contractual	01.01.2016	Actual	01.01.2016
Status	DRAFT		final □	
Nature	prototype □ report **Y** dissemination □			
Dissemination level	public □ consortium **Y**			

Abstract (for dissemination, 100 words)	This report describes the evolution of the sea level and storm surges at the European coast under future global warming climate with special focus at the Greve municipality as case study. A regional atmosphere-ocean fully coupled model has been used to dynamically downscale the CMIP RCP 4.5 and 8.5 scenarios (for medium-low and high GHG emissions, respectively) to obtain detailed sea level patterns at the Northeastern Atlantic and European Seas for the historical and future climate (1960-2100). From these simulations, an analysis of sea level trends and a characterization of extreme high sea level events are carried out.
Keywords	

Version Log				
Issue Date	Rev. No.	Author	Change	Approved by

Contents

1 Introduction

The change of relative sea level is a result of different physical processes. At global scale, total sea level change is induced by ocean thermal expansion due to warming, addition of water from land and ice (mass loss of glaciers and ice sheets). According to the IPCC Fifth Assessment Report (IPCC AR5, 2013) global sea level has increased rapidly in the last decades. Observed global sea level trend shows an increase of 1.7mm yr^{-1} during the period 1901-2010 and 3.2 mm yr^{-1} only for the period 1993-2010. This positive trend is attributed to the effect of warmer temperatures due to the increase in anthropogenic CO_2 emissions. Climate simulations using the Representative Concentration Pathways (RCP) project at the end 21th century (2081-2100) with respect to the historical period 1986-2005 predict a rise of the global mean sea level between 0.26 to 0.55 m for RCP2.6, 032 to 0.63 m for RCP4.5 and 0.45 to 0.82 m for RCP8.5. This rise of the global mean sea level represents a potential risk for human activities and ecosystems mainly at the coastal areas, nevertheless, these trends might not be the same at regional and local scales, where the low resolution of the global models fail in providing adequate information on changing ocean currents and changes in water mass properties. In this report, the sea level signal for historical climate as well as for future climate projections is analysed using downscaling simulations with higher resolution.

The paper is structured as follows:
Section 1: Provides a brief summary and structure of this report.
Section 2: Introduces the modelling tool.
Section 3: Provides a model evaluation of the sea level signal and extreme high sea level events for the recent climate at the European coast.
Section 4: Provides an analysis of the evolution of the sea level and extreme high sea level events for the future climate under global warming conditions.
Section 5: Provides an analysis of the Greve case study.
Section 6: Conclusions
Section 7: Acknowledgments
Section 8: References

2 Modelling tool

2.1 MPG regional coupled climate model

In order to investigate the regional features of sea level change due to ocean circulation and atmospheric loading because of increasing atmospheric CO2 concentrations, the Max Planck Institute for Meteorology has developed a new model set-up to investigate for the European coasts regional sea level rise in transient climate simulations. Downscaling of the CMIP5 scenarios RCP4.5 and RCP8.5 was performed using a regionally coupled model following the approach of Mikolajewicz et al. (2005), Elizalde, A. (2012) and Sein et al. (2015). The ocean component consists of a setup of the global ocean model MPIOM with enhanced resolution around Europe (figure 2.1). The global stretched grid approach allows to adequately capture the short-term sea level signals travelling into the domain of interest. The model uses a bipolar orthogonal spherical coordinate system with a horizontal resolution of 10 km near the coastal areas around Europe and 600 km in the South Pacific Ocean. The model has 29 levels (z-coordinates) in the vertical. The model includes the full luni-solar ephemeridic tidal potential (Thomas et al. 2001).

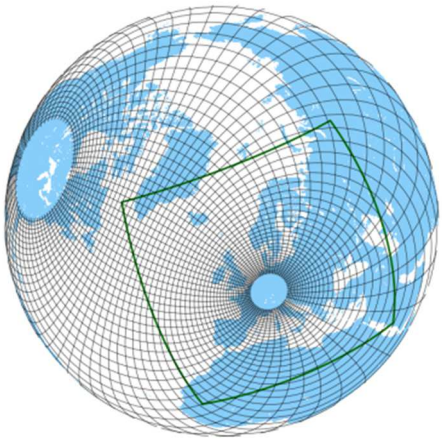

Figure 2.1 Grid and domain areas of the coupled model. The stretched grid of the ocean model is represented by the black lines (not all the mesh is plotted). The green line shows the atmospheric model domain where the models are fully interactively coupled.

Over the European continent and the northeast Atlantic corresponding to the EuroCORDEX domain (Jacob et al,. 2013) extended southwards (see fig. 2.1), the regional atmospheric model REMO is interactively coupled to the ocean model in order to get the benefits of a high resolution atmospheric forcing (figure 2.2). REMO (Jacob D., 2001) is a limited area, three-dimensional, hydrostatic atmospheric circulation model that solves the discretized primitive equations of atmospheric motion. At the lateral boundaries temperature, wind, surface pressure and moisture are prescribed. At the surface boundary, the sea surface temperature is calculated by the ocean model. The horizontal resolution of REMO is 50 km with 27 vertical levels in hybrid coordinates. During the coupling step and in addition to the heat, mass (freshwater) and momentum fluxes, the ocean model is forced with sea level pressure. This allows capturing the full variation of sea level. Outside of the coupling domain, the ocean model calculates the surface fluxes using standard bulk formulas with atmospheric input data derived from the global model. The

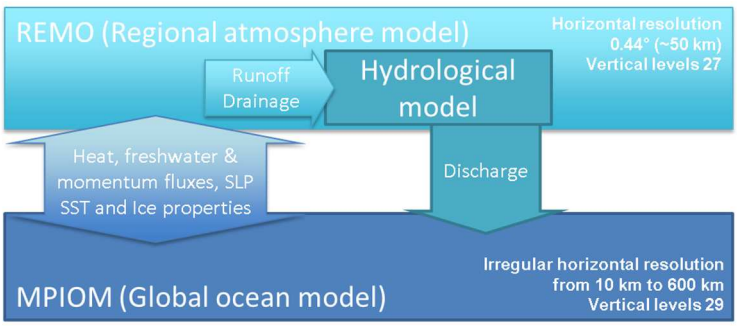

Figure 2.2 Schematic diagram of the regional climate model.

hydrological budget in the study domain is closed using a hydrological discharge model (Hagemann and Dümenil, 1998).

Within the PEARL project a modelling cascade is applied: Data produced by this regional climate model are distributed to the project partners who use them to drive their higher resolution models. This approach allows to investigate the influence of the projected anthropogenic climate change on waves and storm surges at a local scale.

The strategy applied in PEARL to analyse and model the extreme events based on MPG regional model output is as follows:

2.1.1 CAM – Downscaling to very high resolution (10 – 50 m) with LES atmospheric models

Downscaling from regional scale to LES high resolution models - Within PEARL, extrapolation of REMO model data with approximately 50 km resolution to 10 - 50 m resolution will be performed by extracting temporally resolved atmospheric conditions at a particular location from the regional scale model outputs, and using these data as initial and boundary forcing to drive separate high resolution simulations. In this one-way coupling method, information passed to the high-resolution model not only includes standard atmospheric quantities (atmospheric pressure, air temperature, relative humidity and wind speed) but also secondary quantities (fluxes, synoptic divergence, large scale air temperature and moisture tendencies) that must be incorporated to prevent the mean high resolution solution from drifting away from the regional scale prediction.

The ATHAM-Fluidity model - The relative low-resolution data provided by the MPG regional atmospheric climate model, REMO, will be used to drive high-resolution (LES) atmospheric simulations performed by the ATHAM-Fluidity model. ATHAM-Fluidity, a novel high-resolution atmospheric model developed as part of Work Package 2, makes use of advanced numerical techniques to solve the governing equations. The dynamical core is based on the Fluidity solver (Ford et al., 2004) developed at Imperial College London (ICL) and using mixed finite-element methods on fully unstructured, adaptive meshes. The physical parameterizations describing moist atmospheric processes follow mostly the ATHAM model (Oberhuber et al., 1998) developed at the University of Cambridge.

For the one-way dynamical downscaling method described previously, the large scale disparity between the high and low resolution grids (a grid cell of the REMO regional model used here is ~50 km wide, comparable to the total size of a typical ATHAM-Fluidity domain) imply that usable initial and boundary conditions for ATHAM-Fluidity are provided in the form of instantaneous 1D vertical profiles extracted from a single column of the regional model domain. These profiles must then be spatially and temporally interpolated to the high-resolution grid, and possibly adjusted to satisfy specific model requirements. Along the lateral boundaries, the low resolution flow field must be enforced while avoiding the reflection of internally generated physical waves. This is achieved by relaxing the solution field towards the prescribed boundary state from the regional model outputs in layers of finite thickness in the vicinity of each open boundary. At the surface, available land and ocean surface models can be directly coupled to the LES for an interactive evaluation of surface heat and moisture exchanges. In addition to using time varying boundary conditions, it is also often necessary to nudge specific variables towards the time dependent low resolution state. The effect of synoptic atmospheric pressure systems must finally be included through additional sources representing large scale convergence or divergence of the flow field. The latter ingredients are necessary to parameterize the effects of unresolved large scale atmospheric features on the LES solution field.

Methodology - The general framework described above will be used to analyse the local development and impact of heavy precipitation events focusing on two specific case studies: Greve

and Genoa. In both cases, downscaling and the ATHAM-Fluidity model will be used to provide high resolution precipitation maps in the areas of interest. Data generated by ATHAM-Fluidity will be used later on to drive other numerical models part of the integrated modelling framework and focusing, for example, on urban flood modelling.

We worked closely with associated partner 3 (Chinease Academy of Sciences (CAS) and the Institute of Atmospheric Physics in China) to develop an integrated mesoscale and adaptive mesh modelling capability for atmospheric flows. This can be applied at larger scales and was applied to examine pollution dispersion in the mountainous area around Beijing, see Zheng 2015. Here, advanced anisotropic hr-adaptive mesh and discretization numerical techniques were, for first time, applied to modelling of multiscale advection-diffusion problems, which is based on a discontinuous Galerkin/control volume discretization on unstructured meshes. Existing air quality/atmospheric flow models are typically based on static-structured grids using a locally nesting technique. The advantage of the anisotropic-adaptive model is that it has the ability to adapt the mesh according to the evolving pollutant/water vapour/rain distribution and flow features. That is, the mesh resolution can be adjusted dynamically to simulate the transport process accurately and effectively. Comparisons have been made between the results obtained using uniform resolution meshes and anisotropic adaptive resolution meshes. Performance achieved in 3-D simulation of power plant plumes indicates that this new adaptive multi-scale model has the potential to provide accurate air quality modelling solutions effectively.

2.1.2 ICL Storm Surge and Flood modelling

In this project, based on Fluidity-ICOM a new 3D unstructured urban flooding model has been developed. Fluidity-ICOM is an open source 3D unstructured mesh ocean model developed at the Department of Earth Science and Engineering at Imperial College London. It solves the Navier-Stokes equations on arbitrary unstructured finite element meshes. This allows accurate and computationally efficient representation of complex forms. Applying anisotropic mesh adaptivity enables computational resources to dynamically focus on flow complexity, as it develops to reduce computational expense. It includes a single model of ocean basin and coastal zone that is capable of resolving down to building scale and can be used for 3D tsunami and other flooding scenarios (http://amcg.ese.ic.ac.uk/index.php?title =Fluidity).

Using Fluidity-ICOM enables steep topography to be accurately represented along with the associated dynamics unlike classical models. Fluidity-ICOM will be used (without buoyancy forcing) to model coastal zones. The increase in accuracy associated with 3D models can be substantial e.g. in flooding where the vertical inertia cannot be ignored such as where obstructions occur in flowing water. When vertical inertia can be ignored then when one chooses to use a single element in the vertical then there is a constant scalar difference between the speed of a shallow water equation (s.w.e.) model and the 3D model and if one uses a constant basis functions in the vertical then the 3D model and swe's are almost the same with the current formulation. The current formulation (like the s.w.e.'s) puts the free surface variation into the effective pressure variable and thus solves for a single combined pressure and free surface variable making it highly efficient for flooding. These 3D arguments enable one to move from the flood plane to the ocean dynamics within the same model.

In the future more extreme and frequent weather events are expected to take place due to climate change and those events may lead to flooding in urban areas. The main natural hazards causing flooding in urban areas are pluvial flooding and flooding from the sea. The current work focuses on Greve, Denmark. Greve is a coastal city connected to the Baltic Sea via the Øresund belt and traversed by several minor rivers. This city is potentially affected by both of the above mentioned

flood hazards, therefore the performance of an analysis involving the two hazards at the same time would be of great interest (Soledad, 2014).

The principal objective of this research is to achieve urban flooding simulation with the three-dimensional fluid model Fluidity-ICOM in urban areas with storm sewer systems, and its application in the analysis of interactions of pluvial and coastal flooding. More Details can be found in Deliverable D2.2.

2.1.3 TUHH - Assessment of changes of average and extreme wave events due to climate change.

The work at TUHH contributes to the development of the integrated modelling/hazard assessment framework (atmospheric-ocean-waves) including uncertainty assessment and characterisation of extreme events.

TUHH directly uses the near surface wind components of the MPG coupled regional climate model to force a wave model for the area of the Western Baltic Sea (model name "WBSSC"). The wave model is set-up using the 3rd generation spectral wave model SWAN (Booij et al., 1999) with a high temporal (Δt=1 hour) and horizontal ($\Delta x=\Delta y$=ca. 1 km) resolution. Moreover, the wave model runs under sea ice-free conditions and at a mean water level. Since the wave conditions are derived for locations in the Baltic Sea near the 10m depth contour line ca. 1km off the coast (at quasi deep water conditions) the future sea level rise is neglected in the wave simulations. Bathymetric data of the western Baltic Sea originate from Seifert et al. (2001) with a horizontal resolution of ca. 1km.

Wave simulations will be conducted on the basis of near surface wind fields with a horizontal resolution of ca. 50 km and a temporal resolution of 3 hours taken from simulations produced with the MPG coupled regional climate model (see section 2.2).

The changes of the average wave conditions (significant wave heights, mean wave periods and mean wave directions) will be analysed in the entire western Baltic Sea area on the basis of average values of the wave parameters for two scenarios consisting of time periods of 30 years, scenario 2050 (2021-2050) and scenario 2100 (2071-2100).

The changes of extreme wave events will be analysed with a focus on the Greve case study area and for significant wave heights with a return period of 200 years. Annual maximum values of significant wave heights are selected from time periods of 40 years and different extreme value distribution functions (Weibull, Log-normal, GEV, Gumbel) are fitted to the samples by using Maximum-Likelihood estimation.

Finally the uncertainty of the changes of the wave climate will be assessed.

2.2 Regional climate simulations

A set of climate simulations was performed using the MPG regional climate coupled model described in section 2.1. Prior to the production runs, the model was spun up in order to provide adequate initial conditions. The simulated periods comprehend the last decades of the 20th century until the end of the 21st Century.

Validation simulation - In order to assess the model performance in simulating the recent conditions of the sea level, two simulations using 'perfect' boundary conditions were carried out for

the period 1960-2000, one with the fully coupled model and the second with the MPIOM ocean model in stand-alone version. The ERA40 reanalysis data set (Uppala et al., 2005) was used as driving data set.

Historical period – To investigate changes derived from future climate warming, a historical period for the last decades of 20th Century (1960-2005) was simulated as a reference for future climate simulations. As boundary conditions the first realization run (r1lip1) from the global model MPI-ESM-LR (Giorgetta et al. 2013) from the Climate Model Intercomparison Project experiment (CMIP5) was used. The concentration of the greenhouse gases (GHGs) for this period was specified according to observed values.

Scenario RCP 4.5 – For the climate change simulations, a transient run was carried out in the period 2006-2100 as a continuation of the historical period. The same realization run (r1l1p1) from the global model MPI-ESM-LR was used to drive the model. The evolution of the GHGs corresponded to the medium-low emissions scenario Representative Concentration Pathway 4.5 (RCP 4.5) (Thomson et al., 2011).

Scenario RCP 8.5 – Similar to the scenario RCP 4.5, but for the high end scenario RCP 8.5 (Riahi et al., 2011).

Control simulation – In order to account for potential long term deviations between the initial conditions and the mean state of the climate simulated by the model due to model drift, a preindustrial control run of 141 years length was carried out. Any trend derived from this simulation was subtracted from the historical and scenario trends. In this simulation, the atmospheric GHG concentrations were fixed to 1850 values for the entire simulation.

3 Simulation of the recent climate sea level signal

The model's performance simulating the sea level for the present climate is here evaluated. The validation simulation (downscaling of the reanalysis data ERA40) is compared with observation data from satellite and tide gauge stations. Storm surges are studied by analysing the tidal and non-tidal components extracted from the sea level signal.

3.1 Simulation of sea level

The ocean model is able to simulate two of the contributions to the total relative sea level. One of the contributions refers to the increase (decrease) of water volume due to the thermal expansion (contraction) caused by the warmer (colder) temperature oceanic conditions. This is provided as one dimensional variable that contains a global average time series for the simulated period (figure 4.2). The second contribution is what is defined here as the dynamical sea level (DSL) (figure 4.1); it refers to the sea surface height variations due to the atmospheric and oceanic dynamics with respect to the global mean sea level. It is a two-dimensional variable that by definition has a global average of zero.

3.2 Tides

The tidal constituents have been derived from the DSL using a deterministic harmonic solution and compared with the global (E)mpirical (O)cean (T)ide model derived in 2011 by residual analysis of multi-mission satellite (a)ltimeter data (EOT11a) (Savcenko et al., 2012). To evaluate the model performance, a special focus was laid on the North Sea region where the Atlantic tidal waves play an important role in shaping the sea surface height signal as well as other processes like vertical mixing and sediments transport (Gräwe et al., 2014). In the Mediterranean Sea, the Atlantic tidal energy transport going into the basin is rather small due to narrow width of the Strait of Gibraltar.

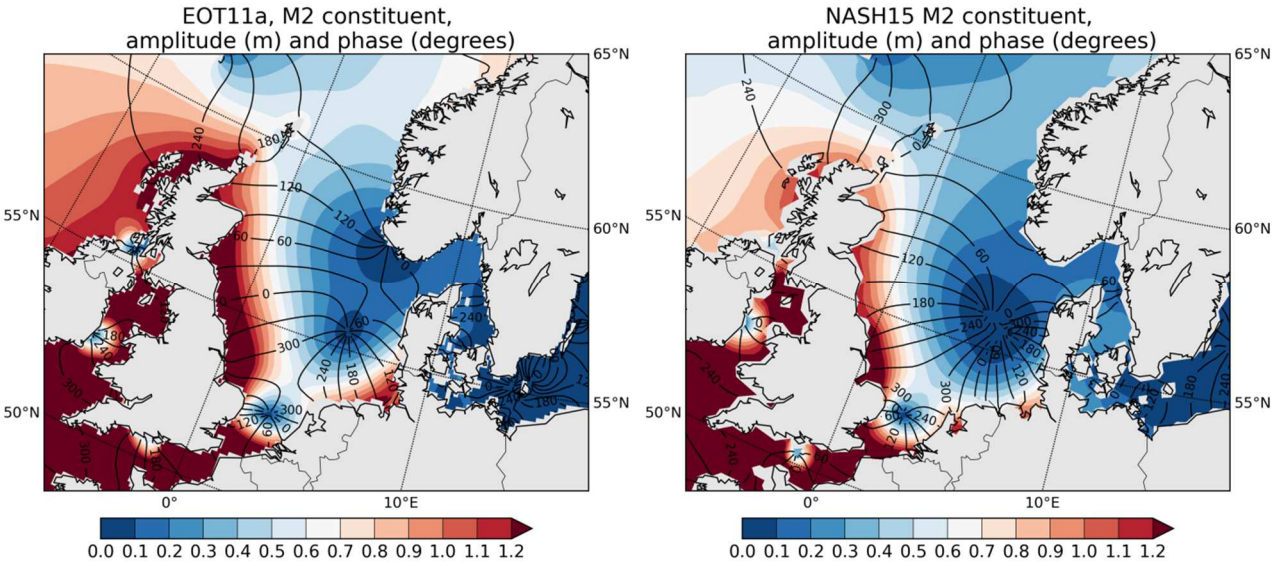

Figure 3.1 Co-tidal plot for the North Sea showing the M2 semi-diurnal constituent amplitude in metre (coloured areas) and co-phase lines in degrees (contour lines) from the EOT11a observation dataset (left) and model (right).

The most relevant tidal constituents at the North Sea are the principal lunar semidiurnal M2, the principal solar semidiurnal S2 and two lunar diurnal tidal constituents K1 and O1 (Roos et al., 2011). Among them, M2 (figure 3.1) is the predominant constituent in the northeast Atlantic due to its large wave amplitude and its effects on the residual currents.

The spatial distribution of the amplitude and the amphidromic system of M2 are well represented by the model. The Atlantic tidal wave traveling eastwards is deflected southwards at the Scottish coast and penetrates into the North Sea basin as Kelvin wave. It travels parallel to the British coast and interacts with the tidal waves entering the North Sea through the Strait of Dover to form an amphidromic point at the German Bight. Its location is well reproduced in the simulation. A second amphidromic point is located over the Dogger Bank as a result of the coastal geometry, topography and Coriolis force influence. The tidal wave propagates anticlockwise along the basin coast reducing its tidal energy due to energy dissipation by the bottom friction resulting in smaller amplitudes along the path. A third amphidromic point is situated near the Norwegian coast. However, its exact location is still under discussion (Sündermann and Pohlmann, 2011; Roos et al., 2011; Davis and Kwong, 2000; Sinha and Pingree, 1997). Even though this point is not present in the simulation, the tidal amplitudes at the Norwegian coast are in the low range close to the observed data and therefore the tides can be considered to be realistic.

Concerning the spatial pattern of the M2 tidal component, the model tends to underestimate its amplitude at the North Atlantic by about 38%. The bias is caused by the low model spatial resolution (10 – 600 km) and the long time step (1080 sec) which the tidal calculation relies on. To investigate this further, a short simulation performed with a higher resolution (5 - 180 km) and a shorter time step (600 sec) was carried out. The higher spatial and temporal resolution shows an improvement not only in the amplitude of the M2 constituent but also in the structure of the North Sea's amphidromic system (not shown). Table 3.1 shows the M2 amplitude averaged over the North Sea ($\bar{A}_{M2}$) and the normalized root mean square error (nRMSE) calculated as the RMSE between the model and observations divided by $\bar{A}_{M2}$. The amplitude bias in the high resolution simulation is reduced to 19% and 43% for the M2 and O1 constituents, respectively. Although, the bias for S2 and K1 increases, the benefits in the improvement on M2 makes recommendable to increase the model resolution to run future experiments. Attempts to perform the experiments with this higher spatial resolution on the IBM machine of the DKRZ were not successful due to the rather slow turnaround. When the machine was decommissioned in September 2015, the simulations had only reached the year 2018 although the numerical experiment had lasted more than a year in wall clock time.

Table 3.1 Averaged observed amplitude (m) and normalized root mean square error (%) of different tidal constituents over the North Sea area using one year of simulation from the coarse and fine resolution versions. The EOT11a data is used as a reference dataset.

	$\bar{A}_{M2}$	Coarse res. nRMSE	Fine res. nRMSE
M2:	0.60	38	19
S2:	0.19	30	52
O1:	0.07	87	43
K1:	0.06	52	57

3.3 Residuals

3.3.1 Data sets

Criteria for the selection of the stations with tide gauge data were the location, the quality, the number of available years and the availability of hourly temporal resolution (table 3.2 and figure 3.2). The selected locations cover most of the European coasts. Where available, data from the exact location or close to the PEARL case study sites were used. The data from the tide gauges were extracted from the GLOSS dataset [IOC, 2012]. Only observational data tagged as 'reasearch quality' (i.e. the gauge data passed a quality control and their time series was homogenized) were used. Station data with at least four years overlapping the simulated period (1960-2000 for the validation) after removing the missing values were selected.

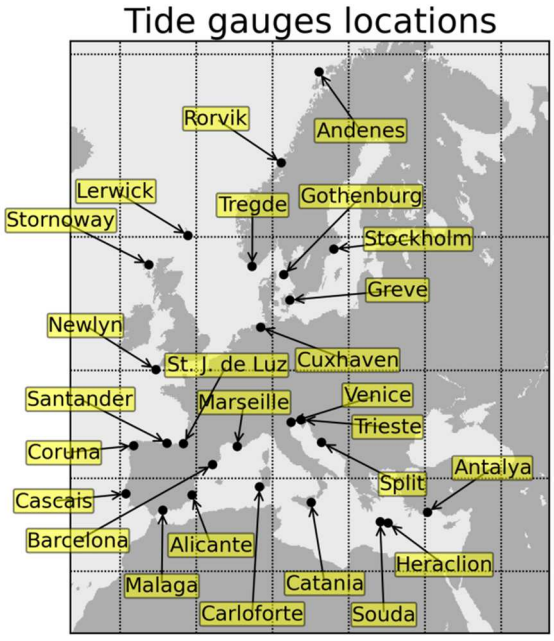

Figure 3.2 Selected stations for the surges analysis

Table 3.2 Overlapping years to the validation simulation period 1960-2000, and number of years used after removing the missing values for each location

Station	Common period	Num. years
Antalya	1985-1998	12
Heraclion	1982-1987	5
Souda	1982-1988	6
Split	1960-2000	41
Trieste	1960-2000	41
Venice	1983-2000	18
Catania	1971-1982	11
Carloforte	1991-2000	5
Marseille	1985-2000	5
Barcelona	1992-2000	8
Alicante	1960-1997	32
Malaga	1992-2000	9
Cascais	1960-2000	38
Coruna	1960-2000	40
Santander	1960-2000	39
St. J. de Luz	1964-1997	32
Newlyn	1960-2000	41
Malin Head	1960-2000	39
Stornoway	1976-2000	21
Lerwick	1960-2000	41
Tregde	1960-2000	39
Cuxhaven	1960-1987	28
Gothenburg	1967-2000	34
Stockholm	1960-2000	40
Rorvik	1969-2000	31

The DSL time series were extracted from the validation simulation of the coupled model by selecting the model grid box that best matches the latitude and longitude of the corresponding station data. Since the horizontal variability of the local sea level is rather small, it is assumed that the sea level of each model grid box represents well the local signal of the sea level and therefore can be directly compared to the station data.

To analyse and validate the model's ability to reproduce the surge events, the non-tidal component or residual is obtained by subtracting the astronomical tides component from the detrended sea level signal. This calculation is applied separately to both DSL model time series and sea level gauges station data. The astronomical tides are calculated using a deterministic harmonic analysis method implemented in the T_TIDE Matlab package (Pawlowicz et al., 2002).

The variability of the residuals is investigated at intra-monthly, seasonal and interannual frequency bands. A filter (running mean) is applied to separate the 1-30 days signal (storms to intra-monthly processes). The seasonality is calculated as a climatology from filtered intra-monthly time series, which is then subtracted from the former to obtain the inter-annual signal. Figure 3.3 depicts the variability (the variance of the time series) as a percentage for each component relative to the variability of the DSL signal for model (lines) and detrended sea level observational (bars) data.

The tidal component explains most of the sea level variability at the locations in the Atlantic coast. The simulated tidal variability of all the locations at the Atlantic, North Sea, Kattegat and Norwegian coasts is in a very good agreement with observations. The Mediterranean Sea is a semi-closed basin in which the tidal energy is limited to the influence of Atlantic tides and its own basin-generated tides. Given the narrowness of the Strait of Gibraltar, that connects the Atlantic ocean with the Mediterranean Sea, the Atlantic tidal energy has a limited influence over the western basin and the basin-generated tidal energy is relative weak given the relative small size of the basin. Therefore, the variability of the tides explains only about 4% to 40% of the detrended sea level variability, with an exception of the north Adriatic Sea (Trieste and Venice stations) where approximately 80% of the sea level variability is a consequence of the resonance of the basin-generated tides from the eastern basin. The model simulates well the spatial distribution of the tides variability in the Mediterranean Sea, in particular the variability at the north Adriatic. Nevertheless, a somewhat too high tidal energy generates a larger variability for some of the stations.

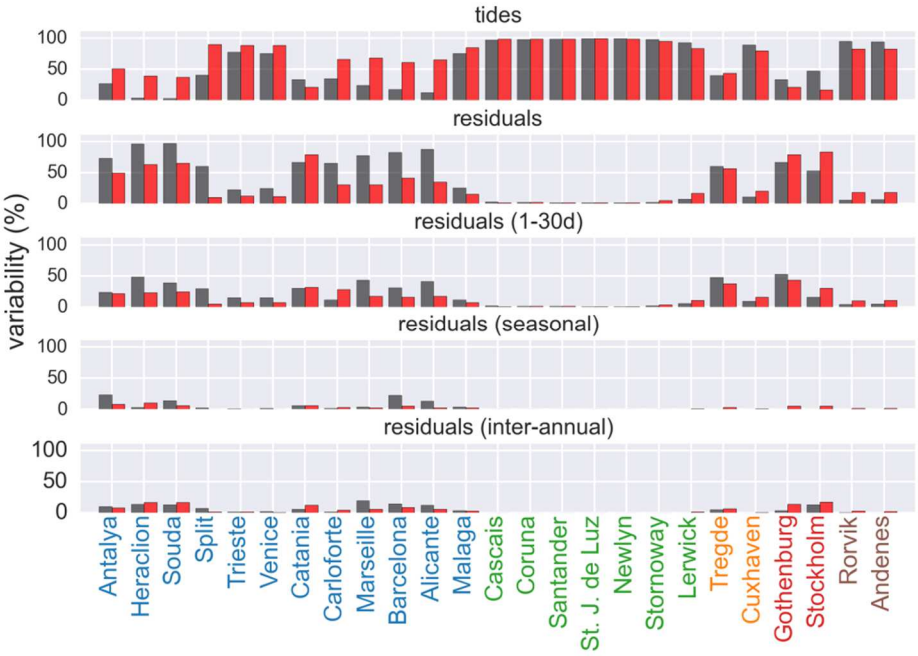

Figure 3.3 Relative variance of tides, residuals and different temporal frequency bands for residuals expressed as a percentage relative to the variance of variability of the detrended sea level signal for different locations at the European coast. Mediterranean (blue), Atlantic (green), North Sea (orange), Kattegat and Baltic Sea (red) and Norwegian Coast (brown). The bars in red correspond to model data and in grey to observations.

In accordance with observational data (figure 3.3), the variability of the residuals at the Atlantic is rather low approximately from 1% to 7% of the detrended sea level variability. At the Baltic and Norwegian coasts, the variability is larger reaching up to 65% depending on the location. Most of this variability is related to intra-monthly storminess at the Tregde and Gothenborg stations with a contribution of around 50%. At the Mediterranean Sea, the variability of the residuals explains from 60% to 97% of the variability of the detrended sea level variability. The intra-monthly signal contributes to explain 10% - 50% of the detrended sea level signal followed by the 2%-20% of the inter-annual variability and 1% - 23% from the seasonal signal. In the different frequency bands of the residuals, the model is in a very good agreement with the variability across the European coast. This implies a good representation of the contribution not only of the short term effects by the atmospheric processes but also by the seasonal steric component and atmospheric seasonal cycle, and by the large-scale inter-annual atmospheric circulation.

The model biases for the residuals with respect to the observed tide gauge data are shown in figure 3.4 in terms of the temporal correlation and the root mean square error relative to time series one standard deviation. There is no a particular spatial pattern in biases of the residuals. The correlation is typically in the range of 0.5-0.8 (except for the Antalya and Carlofonte stations) which is comparable to correlations of 0.8 obtained by using storm surge models (sea level estimates based on atmospheric-induced effects only, no ocean circulation and thermal expansion effects are included) at the Mediterranean region [Androulidakis et al., 2015]. The relative error is in the range of 70%-110% (with exception of Stockholm, Antalya and Carlofonte stations) with a better performance at the Spanish coast. These values are relative high if compared with 20%-40% biases shown for surge models [Androulidakis et al., 2015, Conte and Lionello, 2013]. However, these results can be considered as a good achievement of the coupled climate model taking into account that a new degree of freedom is introduced at the air-sea interface within the coupled area. In addition, surface processes are not either bounded or driven by any forcing dataset. For simulations of future changes of sea level (especially the changes due to steric sea level changes) a climate modelling set up is required, a pure surge model would not be sufficient.

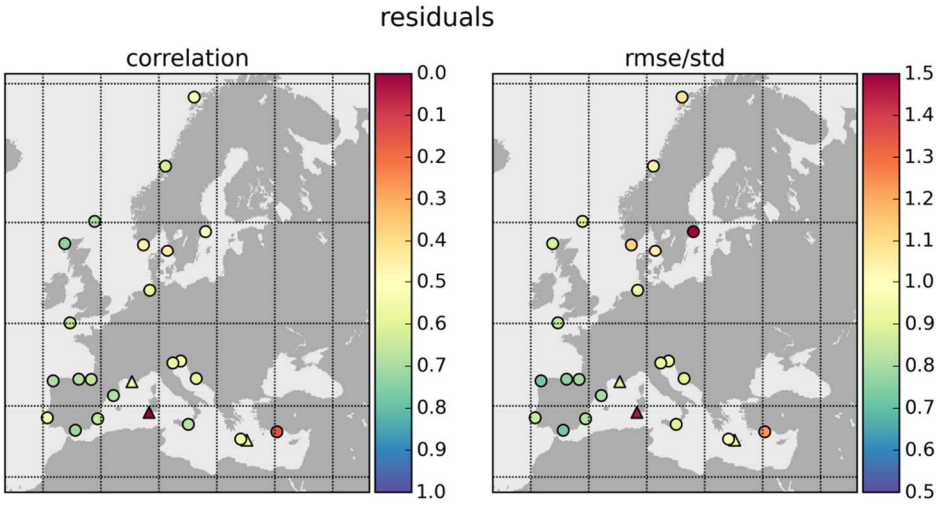

Figure 3.4 Correlation (left) and error relative to the variation (right) of model with respect to observations for the residuals. Triangles indicate locations with time series shorter than 5 years

3.3.2 Extreme sea level events

The likelihood of the occurrence of extreme sea level events (referred to as “storm surges”) is correlated with the North Atlantic Oscillation (NAO) index in the winter-mean timescale on the northwest of Europe (Wakelin et al., 2003). At the North West Atlantic and North Sea coast, the extreme sea level events are related to the direction and speed of the wind that is determined by the low pressure systems travelling in south-eastward direction towards northwest Europe (Woth et al., 2005). In the Mediterranean Sea, storm surges are highly correlated with the NAO at the western and central coasts of the basin, whereas at the eastern basin the correlations with the NAO are weaker (Marcos et al., 2009).

In order to investigate the model’s performance simulating the extreme sea level values produced in a free air-sea interaction, the validation simulation of the coupled model was compared with the uncoupled version forced with the same reanalysis dataset (ERA40). The ocean component of the coupled model benefits from the free air-sea interaction and a higher spatial and temporal resolution of the surface forcings (the coupled model atmosphere forcings has a spatial resolution of 0.44° x 0.44° degrees and 3 hours coupling time step compared with 1.25° x 1.25° degree and 6 hours forcings in the uncoupled version). Figure 3.5 shows the extreme values of the non-tidal component of the DSL calculated as the 99th percentile and the 100y return level (RL_{100y}) values for the coupled and uncoupled model data (driven with reanalysis forcings) as well as for detrended sea level of the tide gauge stations from the GLOSS dataset (IOC, 2012). The RL_{100y} value is calculated inferring the Generalized Extreme Value (GEV) distribution from the r-largest extreme sea level events per year (in this case 10 maximum values per year in the available common years between DSL model and the detrended observations within the period 1960-2000 were used, see Table 3.2). The log-likelihood function maximization is used to estimate the distribution parameters to fit the theoretical distribution to the empirical one. Location data that did not converge when fitting the likelihood function were excluded from the return level figures. The confidence intervals (CI) are computed applying the bootstrapping method based on 1000 resampling iterations with replacement at a 95.45% confidence limits; two standard deviations of the estimators derived from the likelihood function maximization.

The spatial distribution of surge maxima is well reproduced in both model simulations. The coupled model is able to simulate higher extreme values due to the finer spatial resolution of the surface forcings and the active air-sea interaction that influences the driving mechanisms of storm surge formation such as the magnitude of the wind speed and the spatial pattern of the atmospheric pressure. This advantage can be seen in regions of complex orography like in most of the stations at the Mediterranean coast in particular at the North Adriatic Sea where strong wind events sustained over time can increase temporarily the sea level by piling the water against the coast.

In contrast to the 99th percentile, for the RL_{100y} value calculation only the maxima within the time series are selected (i.e. it gives a general information of the characterization of the maximum values of the time series only, not the whole time series). Both model versions reproduce the observed maxima quite well. Confirming the 99th percentile results, the coupled model simulates larger values particularly at the Atlantic coast. Cuxhaven and German North Sea coast are exceptional cases of large values of storm surges in the North Sea by the superimposition of water masses build-up and astronomical tides. In this case, the estimated 100 year return value from observations is 523 cm which is similar to 507 cm ± 30 cm calculated by Mudersbach and Jensen, 2010 using a similar method but a longer time series (1849-2007). The large CI of the Cuxhaven station plotted in figure 3.5 are derived from the large variability of the local sea level and the relative short time series of 28 years in common between observational and simulated sea level time series (table 3.2). Based on the results from our calculations we conclude that the uncoupled model underestimates the return period but that the coupled model agrees well with the range of the RL_{100y} estimates.

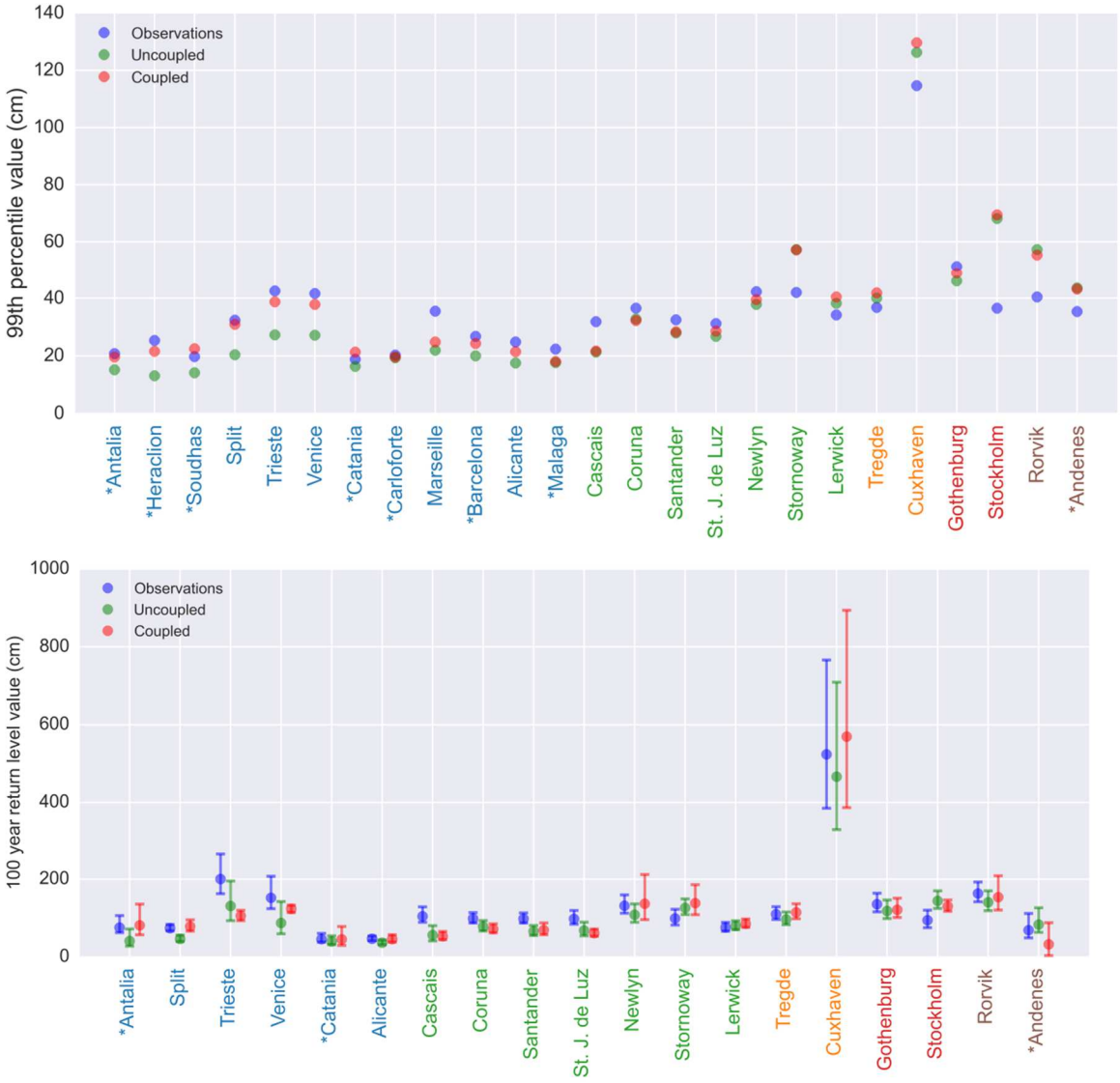

Figure 3.5 99th percentile (top) and 100 year return level values with 95.45% confidence intervals (bottom) for the simulated surges and observations data. The asterisk indicates locations with time series shorter than 15 years. Location colors are the same as figure 3.3.

4 Sea level evolution under climate change

4.1 Total relative sea level

The sea level rise signal due to the effects of ocean circulation and atmospheric pressure changes in response to anthropogenic climate change has been analysed. Additionally, the trend of the total relative sea level (RSL) is calculated by adding to the former the contribution from the global thermal expansion simulated by the model plus the signal from changes in the cryosphere and the land water storage. The 1960-1990 period from the historical period and the 2070-2100 periods from the RCP4.5 and RCP8.5 scenarios have been analysed.

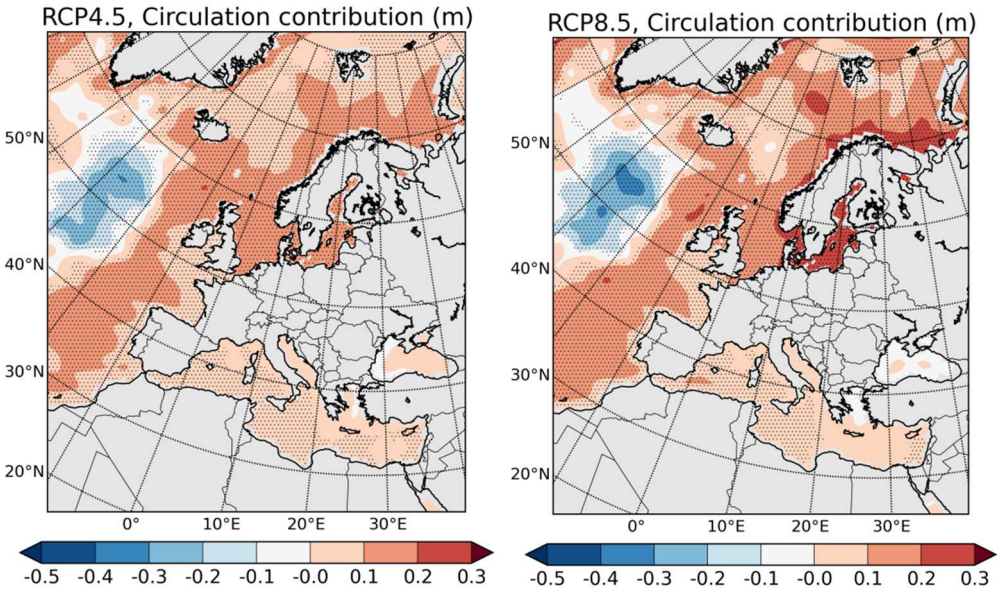

Figure 4.1 Contribution to the sea level induced by oceanic circulation, ocean thermal expansion and atmospheric pressure load for the last decades of the 21th century (2070-2100) in reference with the historical period 1960-1990 for the climate scenarios RCP4.5 and RCP8.5. Significant values at the 99.9% level are indicated by dotted areas.

The changes of DSL due to changes in oceanic circulation, ocean thermal expansion and atmospheric pressure load at the end of the 21st century with respect to the recent past climate as simulated by the model are represented in figure 4.1. The model simulates a general increase of more than 0.1 m for almost all northern and central European coasts for both scenarios (RCP4.5 and RCP8.5). In particular, an increase up to 0.28 m around Scandinavia and the Baltic Sea is simulated in the scenario RCP8.5. The strong increase in the Baltic is a consequence of the simulated reduction in salinity due to enhanced river inflow and precipitation. The outflow of freshwater from the Baltic is enhanced leading to a strengthening of the low salinity component of the Norwegian Coastal Current and thus to a stronger rise in total sea level along the Norwegian coast. Within the Mediterranean Sea, the sea level increases less than the global mean due to enhanced net evaporation and thus an increase in the simulated salinity. This effect is strongest in the eastern Mediterranean, where the total sea level rise reaches a regional minimum.

The decrease of the simulated total sea level height shown at the Atlantic region (blueish area in figure 4.1) corresponds to an eastward expansion of the North Atlantic subpolar gyre, which is driven by changes in wind forcing.

The global thermal expansion contribution due to ocean heat uptake including the deep ocean is shown in the figure 4.2. For the present climate period 1993-2010 a rise rate of 2.02 and 1.88 mm yr-1 is simulated in the RCP4.5 and RCP8.5 scenarios, respectively. In accordance with the uncertainty range from observations from 0.8 to 1.4 mm yr-1 the model tends to overestimate the trend. It can be seen in the figure 4.2 that in 1993 our model has a local minimum in the interannual variability of thermal expansion, thus the trend estimated from our model for this period is biased towards high values. However, the rates are within the interval of 0.97 to 2.02 mm yr-1 simulated by the CMIP5 models in the same period (IPCC AR5). The projected global mean sea level rise increases in 2081-2100 relative to the 1986-2005 by 0.21 m (RCP4.5) and 0.30 m (RCP8.5) in a good agreement with estimates given in the IPCC AR5 (0.14 to 0.23 m and 0.21 to 0.33 m for RCP4.5 and RCP8.5, respectively) (Stocker et al. 2013). Since the area outside of the coupling region is driven directly by the MPI-ESM-LR model, values similar those from the MPI-ESM-LR model for the thermal expansion were expected in our simulations.

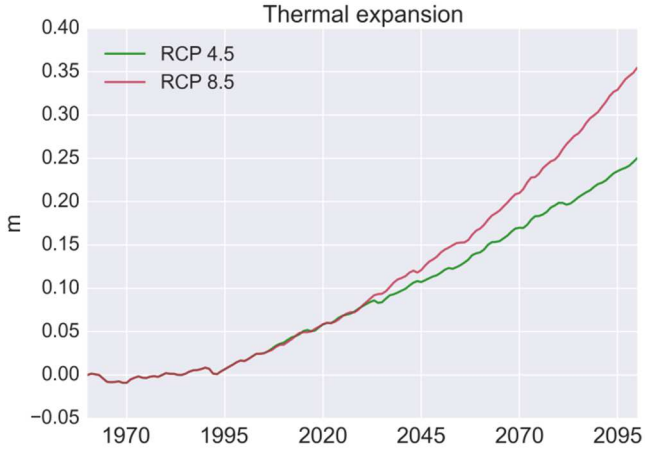

Figure 4.2. Simulated steric height contribution to the global sea level

The contributions from cryosphere and land water storage to sea level rise are not included in our regional model system. These contributions have been estimated using other setups of the MPI-M model system wherever possible. As these are not spatially uniform, the spatial sea level patterns for the individual components by Bamber and Riva (2010) have been used. The mass loss of the Greenland ice sheet due to anthropogenic climate change was taken from Vizcaino et al. (2015, using an ice sheet model interactively coupled to the MPI AOGCM). The contribution of the smaller glaciers was taken from Marzeion et al. (2012) who used the same MPI-ESM-L-r1l1p1 simulation as in our experiments to drive their glacier model. For Antarctica as well as for the future evolution of water storage on land estimates from Church et al. (2013), (IPCC report chapter 13) have been used. For the long term effect of glacial isostatic adjustment the ICE-5G estimates (Peltier 2004) have been used. The latter effect is responsible for the strong rise of land in northern Scandinavia (up to 1m/century), leading to a local reduction of relative sea level. Similar but smaller signals can be seen in Scotland and Iceland, whereas the land around the southern North Sea is sinking. The glacial isostatic adjustment is a consequence of the climate changes since the last glacial maximum (21000 year ago) and independent of anthropogenic climate change.

The horizontal distribution of the contributions to relative sea level, which is not included in our climate model (cryospheric and land water storage, glacial isostatic adjustment), is shown in figure 4.3. This signal is comparable in magnitude to the oceanic and atmospheric contribution shown in figure 4.1. For large parts of the European coast line sea level increases between 0.2 to 0.4 m. The negative trend of RSL at the coast of the Scandinavian Countries, Iceland, Greenland in northern Barents Sea is a consequence of the land masses rebounding after the last glacial period.

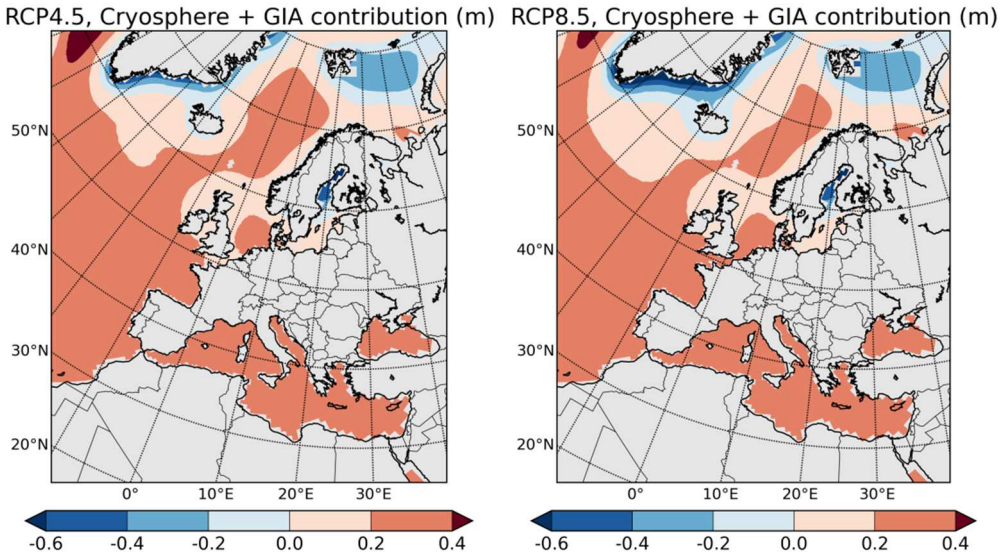

Figure 4.3 Regional contribution to relative sea level from the Greenland and Antarctic ice-sheets, smaller glaciers and ice caps and the glacial isostatic adjustment (GIA) calculated for the last decades of the 21th century (2070-2100) for the climate scenarios RCP4.5 and RCP8.5

As mentioned earlier, the total RSL change is calculated as the sum of all the previous contributions (figure 4.4). In general the total RSL rise for the along European coast including the Mediterranean and Atlantic coasts is in the range of 0.4 to 0.6 m and 0.4 to 0.8 m during the last decades of the 21th century (2070-2100) for the climate scenarios RCP4.5 an RCP8.5, respectively, with respect to the average of the historical period 1960-1990. The maximum sea level rise of the European coast in both scenarios is obtained in the south-eastern North Sea. Most of the spatial pattern of the distribution at the North of the European continent is dominated by the cryospheric effect and the glacial isostatic adjustment. A sea level fall in the range of -0.6 to -0.2 m and -0.4 to -0.2 m is projected at the coast of northern Scandinavia as a consequence of the glacial isostatic adjustment for the RCP4.5 and RCP8.5 scenarios, respectively.

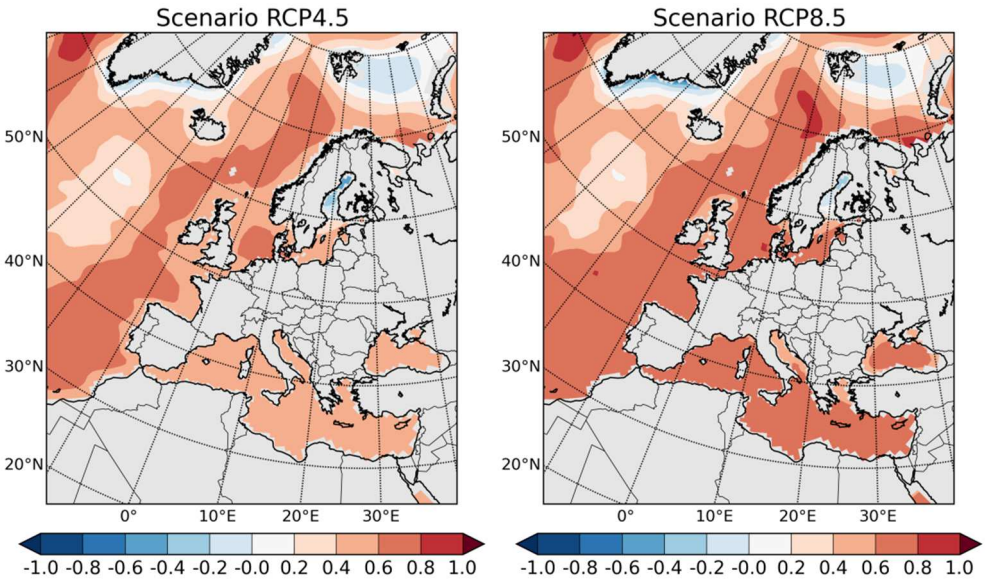

Figure 4.4 Total relative sea level increase (m) in the last decades of the 21th century (2070-2100) of the climate scenarios RCP4.5 an RCP8.5 with respect to the average of the historical period 1960-1990.

4.2 Variability of the residuals

The residuals of the transient climate simulations have been obtained by subtracting the tidal component to the sea level time series (i.e. sea level or DSL signal from the oceanic circulation, the ocean thermal expansion and atmospheric-induced effects), similar as for the model evaluation. The data have been filtered in three frequency bands (intra-monthly, seasonal and inter-annual) (see section 3.3.1) for the historical period (1960-1990) and both future climate scenarios (2070-2100). The atmospherically-induced effects modify regionally the variability of the residuals and frequency bands up to 5% in the future climate with respect to the historical period (not shown). For the inter-annual variability, the RCP 8.5 scenario has a reduction up to 5% in the variability over the Mediterranean Sea and slightly increase up to 3% at the north European locations with respect to the past climate (in the RCP 4.5 scenario these values are -3% and +3%, respectively). These changes are attributed to the difference in the spatial pattern of the simulated mean sea level pressure (MSLP) between both periods (Geng and Sugi, 2003; Zappa et al,. 2013). Model results show a north-south gradient in MSPL change across Europe from -2 hPa in northern Scandinavia to 1 hPa over the southern European countries. In accordance with the more frequent high pressure systems in southern Europe, the storm tracks trajectories are shifted northwards. As a consequence, the storminess in northern/southern Europe is increased/decreased. After applying the Levene statistical test to compare the variances of the time series of the residuals, the changes in the residuals and in the different frequency bands turned out to be significant at 95% confidence interval. This results confirms the findings by Marcos et al., 2012 for the Mediterranean region using A1B and A2 SRES climate change scenarios.

4.3 Changes in the surges

The 99th percentile and 100 year return values of the residuals for historical and future periods (figure 4.5) were calculated with the same procedure as for the model validation (see section 3.3.2). These data are calculated relative to the mean sea level. Similar to the previous subsection, the spatial distribution of the 99th percentile values can be explained not only by the poleward shift of the storm activity in the projected climate but also by regional changes of the storms intensity. The increased north-south MSPL gradient induces stronger geostrophic winds in the surroundings of the low pressure core resulting in larger extreme sea level values at higher latitudes in the European region. The opposite effect takes place in the southern region where the extreme values decrease due to a reduction in storms activity. These results confirm the findings by other authors (Marcos et al.,2012; Jorda et al., 2012) who conclude that atmospheric-induced effects have less influence on the storm surges over the Mediterranean region. In general, these mechanisms are more pronounced in the RCP 8.5 scenario than in RCP 4.5. The results of RL_{100y} values calculated from the climate projection show larger probabilities of stronger storm surges in the projected climate, particularly for some of the stations located at the Atlantic. For the Mediterranean Sea, the weakening of storm surges indicates that the effects of the storm intensity are regionally dependent. However, none of the changes is statistically significant for the analysed locations.

It is here important to note that extreme values refers to detrended none-tidal component of the DSL signal, i.e. surges derived from the atmospheric-induced effects only. To obtain the real extreme RSL, the mean change in RSL from section 4.1, which in most places dominates, the trend of the DSL and the tidal component have to be added to the extreme values of the surges.

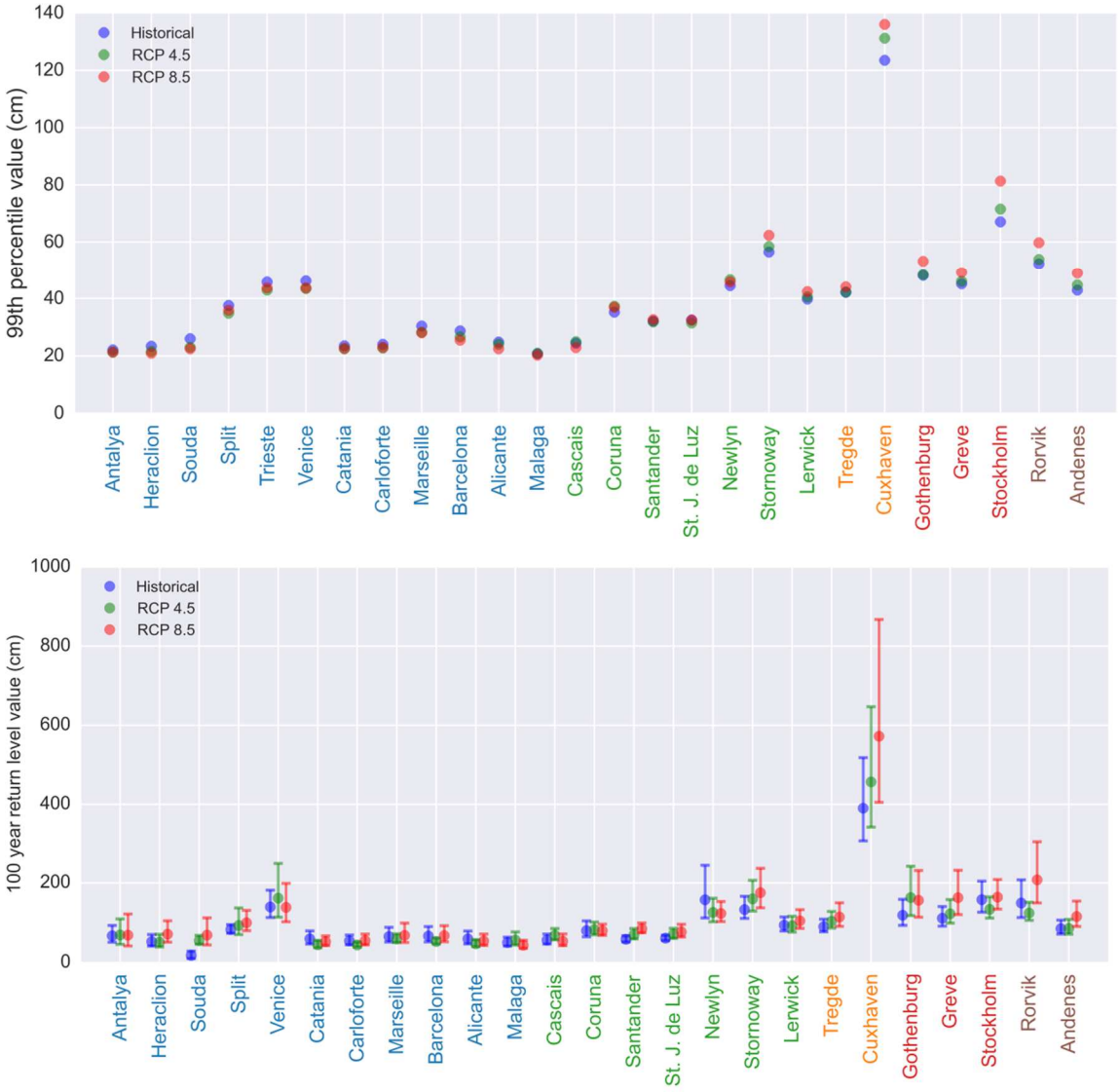

Figure 4.5 99th percentile (top) and 100 year return level values with 95.45% confidence intervals (bottom) for the residuals from the historical period (1960-1990) and both scenarios RCP4.5 and RCP8.5 (2070-2100). Location colors are the same as figure 3.3

5 Greve case study

Greve municipality was chosen as the case study where all modelling tools used and developed in the PEARL project are applied. The municipality covers an area of 60 km^2 and it is located at the Øresund (the easternmost of the Danish Straits) about 21 km southwest of Copenhagen. The straits have a complex topography and given their narrow nature the global models from the CMIP5 exercise do not describe or describe poorly the Baltic Sea and the Danish Straits due to their coarse spatial resolution of approximately 100 km x 100 km at the straits. Thus, the downscaling of the CMIP5 scenarios with our modeling tool with up to 19 km x 19 km resolution at the Danish Straits becomes useful to investigate the sea level evolution under anthropogenic climate change conditions for the Greve site.

5.1 Evolution of sea level rise

Eastern Denmark is influenced by land uplift due to the glacial isostatic adjustment. In the city of Copenhagen the land uplift is about 1.2 mm yr^{-1} (Hallegatte et al. 2008). However, the increment of the global sea level by the thermal expansion, water mass addition due to negative mass balance of the cryosphere and regional changes of the oceanic and atmospheric circulation associated with anthropogenic climate change more than compensates the negative trend of the glacier isostatic adjustment at the Greve location, thus leading to positive values of RSL change. A positive trend of 0.4 mm yr^{-1} of the total relative sea lev el (RSL) is calculated for the decades 1960-1990 in the model. This trend agrees well with the 0.44 mm yr^{-1} from observations that have been reported for the city of Copenhagen (Hallegatte et al. 2008).

Extreme high stands of sea level of 154 cm (in 1902) and 157 cm (1921) above normal sea level have been recorded for the city of Copenhagen. Hallegatte et al., 2008 obtained a 150 cm 100y return level (RL_{100y}) value using a Peak Over Threshold approach based on a long time series 1890-2007 of gauge data for the Copenhagen harbour. For the simulated historical period, the RL_{100y} calculated is 122 cm near the location of Greve (table 5.1), nearly 30 cm lower than the value calculated by Hallegatte et al., 2008. This difference is not unexpected given the limited number of years available in the historical period (1960-1990) and due to the fact that the model did not simulate such observed extreme high water levels from the early 20th century.

Table 5.1 Mean, standard deviation, 99th percentile, and100 years return level with 95.45% confidence intervals for the total relative sea level and statistic of the 5 highest sea level events per year (in cm)

	Total relative sea level					5 highest sea level events per year			
	mean	std	p99%	RL100y	95.45% CI	mean	std	p99%	max
HIST (1960-1990)	0.0	22	52	122	[106 - 145]	64	9	97	105
RCP45 (2070-2100)	57	23	111	191	[169 - 224]	122	9	161	176
RCP85 (2070-2100)	74	24	135	273	[214 - 378]	143	12	187	214

The models shows at the end of the 21st Century (2070-2100) for both climate change simulations an increase of the total RSL with respect the reference period 1960-1990. In the high end RCP 8.5

scenario the rate of projected RSL rise is 8.9 mm yr^{-1}, while it is 3.7 mm yr^{-1} in the moderate RCP 4.5 scenario. The resulting sea level rise averaged for the period 2070-2100 (relative to the reference period) is 0.74 m and 0.57 m for the scenarios RCP 8.5 and RCP 4.5, respectively (table 5.1). Notice that the temporal evolution of the sea level rise is not linear. The faster rise rate for RCP 8.5 is caused mainly by an increase of thermal expansion and contributions from water mass additions. The contribution of the ocean and atmosphere dynamics in this period is 0.23 m and 0.15 m for the RCP 8.5 and RCP 4.5 scenarios, respectively.

5.2 Storm surges

The atmospheric mechanisms leading to the formation of surges in the area of interest are linked to low pressure systems travelling eastwards into the Scandinavian region. The associated southward Ekman transports lead to high sea level stands in the south of the Baltic Sea and Kattegat (Hallegatte et al., 2008). In combination with the decrease in atmospheric pressure load this can cause extremely high water levels in the region. Particularly in south of the Baltic Sea, a low pressure core displacement can also combine consecutive northwesterly and northeasterly winds that produces high water events (Feister et al,. 2003) by the excitation of seiches in the Baltic.

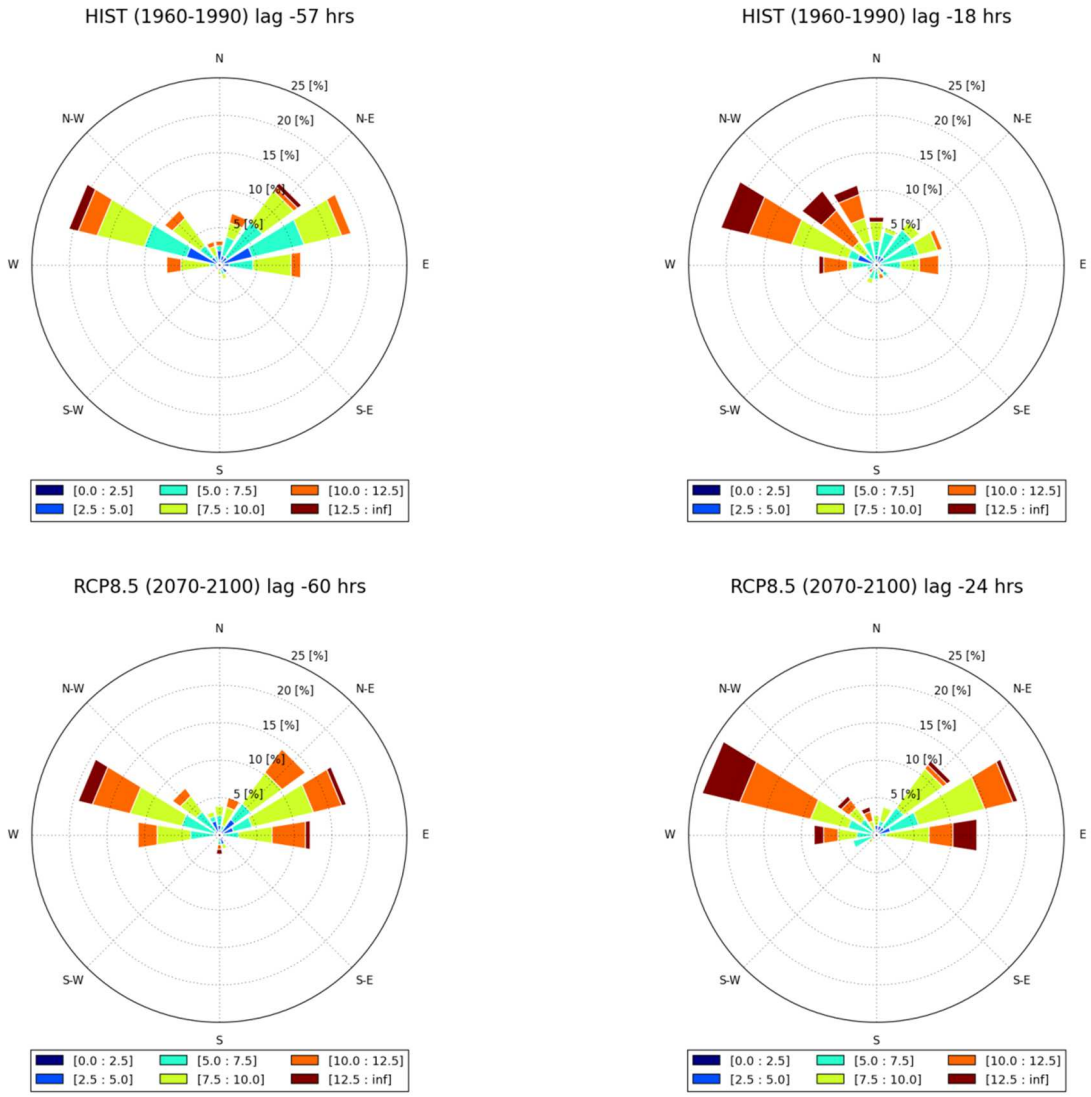

Figure 5.1 Frequency of occurance of the wind direction (%) and wind speed (m s^{-1}) corresponding to lagged wind conditions to surge events at Greve averaged over the periods 1960-1990 for the historical climate and 2070-2100 for the RCP8.5 scenario. The negative time values correspond to two time-lag correlation maxima between surges and wind speed time series.

To investigate the effects of changes in ocean circulation, the ocean thermal expansion and atmospheric-induced processes on surges (extreme high water levels) at Greve, a time series for storm surges is created by selecting the five maximum values per year from the DSL simulated by the model. The surges time series is time-lag correlated with the 3 hourly averaged wind speed time series at Greve's location. This lagged correlation shows two maximum correlated times. The wind direction averaged in a 9 hours window centred at the maximum time-lagged correlation for each of the episodes is depicted in figure 5.1. In the historical simulation, the first local maximum correlation occurs in average 57 hours before the extreme sea level event. The predominant wind directions are from the northwest and northeast with similar frequency of occurrence. The second correlation maximum occurs in average 18 hours prior to the surge event with stronger westerly or northwesterly wind direction up to 25% more frequent wind speeds over 10 m s^{-1} than the easterly winds. These results agree well with the wind driven high water mechanisms described by Feister et al. 2003 and Hallegatte et al., 2008.

The simulations of the projected future climate scenarios do not show changes in the wind direction associated with the occurrence of surges, but in the intensity of the wind. The frequency of winds associated with extreme high water levels with speeds above 10 m s^{-1} and 12 m s^{-1} in the high emissions scenario (RCP 8.5) increases by 10% and 6%, respectively (but not statistically significant). This is in accordance with the effects of the poleward shift of the atmospheric circulation as discussed in section 4.2. In in our future climate simulation the storm activity slightly increases for northern Europe, increasing not only the intensity but also the frequency of storms. As a result, the mean of the five strongest storm surges per year increases by 58 cm and 79 cm (table 5.1) at the Greve site for the last decades (2070-2100) of the 21th Century for the RCP 4.5 and RCP 8.5 scenarios, respectively.

Loew et al. (2005) found that taking into account the total RSL, the 50 yr return period storm surge event (RL_{50y}) becomes 40 – 60 cm higher than today around the western coast of Denmark by the end of the Century for the A2 SRES emission scenario (from the medium-high emission scenarios family). In our case the changes of the RL_{50y} values calculated from the total RSL are lower than Loew's values, 67 cm and 133 cm higher than the historical period for the RCP4.5 (medium-low emissions) and RCP 8.5 (high emissions) scenarios, respectively. The changes of the 100 yr return period are 69 cm and 151 cm for RCP4.5 and RCP8.5, respectively.

6 Conclusions

The main contribution of the MPG to the PEARL project consists in performing a dynamical downscaling of future climate scenarios and an analysis of the sea level trend in such scenarios with a special focus in the extreme high sea level events at the Greve case study. Additionally, the model output produced in simulating future climate projections is been distributed and utilized by PEARL project partners as driving conditions for their models following the model cascade developed with in the PEARL project.

In this analysis, the projected evolution of sea level and storm surge intensities at the European coast under future global warming climate conditions is investigated. A novel approach has been used to model the sea level. Simulations for present and future climate (1960-2100) have been carried out at the Max Planck Institute for Meteorology. The RCP 4.5 and 8.5 scenarios (for medium-low and high GHG emissions, respectively) as simulated by the global model MPI-ESM-LR-r1lip1 have been dynamically downscaled using a regional fully atmosphere-ocean coupled model in order to obtain detailed sea level patterns for the European region.

The comparison of the simulated sea level variability with tide gauge data gave satisfactory results. The astronomical tides and residuals components were computed from the sea level signal. The validation run shows a good agreement with the observed spatial structure of the variability for the tides and the sub-monthly, seasonal and inter-annual frequency bands of residuals. The time correlations are also within an acceptable range if compared with similar analysis using storm surge models. The storm surges computed as the 99th percentile value and the 100 year return period of the residuals using the model data are in a good agreement with the observations not only in magnitude but also in the spatial distribution of the storm surges which give us confidence in the representation of storminess within the model.

The changes in total relative sea level was estimated accounting forfor all sea level contributors, i.e. ocean and atmospheric circulation, thermal expansion of the ocean, the water mass addition from ice sheets and glaciers, land water storage and the glacial isostatic adjustment. Including results from both RPCs scenarios, at the last decades of the 21th century (2070-2100) the simulated total relative sea level increases between 40 and 80 cm at the coastal area of the Mediterranean Sea, Western Europe and the North Sea relative to the reference period 1960-1990. The thermal expansion and the water mass addition by ice-melting dominate the signal at the European coast except for northern Scandinavia where the land rebound due to the glacial isostatic adjustment decreases the sea level approximately 20 to 60 cm. The trends of the simulated total relative sea level in the model are in a good agreement with studies reported in the AR5 IPCC.

In our simulation, the poleward shift of the atmospheric circulation in the projected climate with respect to the historical period implies statistically significant changes in the DSL variability. At the north of Europe, the variability of the DSL increases by about 3% for both scenarios and decreases for the Mediterranean region by 3 to 5% (RCP 4.5 and RCP 8.5, respectively). The variation of the magnitude of the surges produced by storm activity is in agreement with the changes in the MSLP. The extreme values computed as the 99th percentile values of the residuals (DSL without tides) increase by about 5 cm at the northern European coast and decrease around 3 cm in the Mediterranean region relative to the long term mean sea level. Both trends are statistically significant. The 100 year return values calculated from the surges are on average by about 10 cm higher in the north of Europe, but this result is not statistically significant. For the Mediterranean region, no trends in the 100 year return values have been found. These results are in agreement

with the analysis from other authors (Woth et al., 2005; Marcos et al., 2012; Jorda et al., 2012; Androulidakis et al., 2015).

For Greve municipality, the projected mean sea level for the decades 2070-2100 of the RCP 4.5 and RCP 8.5 scenarios becomes approximately 60 to 75 cm higher, respectively, than historical levels in the decades 1960-1990. Concerning the storm surges, the wind direction that induces the extreme high water levels at Greve does not change in the climate projections. However, the northwesterly and northeasterly winds related to storm surges become more frequent and intense in both RCPs scenarios because of the increment in the frequency of the cyclone activity at northern Europe. The RL_{100y} of the total relative sea level in the future climate increases approximately 70 cm with 95%CI of [24-118] cm and 150 cm with 95%CI of [69-272] cm for the RCP 4.5 and RCP 8.5 scenarios, respectively, with the historical period as a reference. This implies that approximately 10 cm and 75 cm, respectively, are explained by the changes on the atmospheric load and ocean dynamics. Despite the fact that these changes found to be not statistically significant the values are consistent with the results from other authors; Woth et al. 2005 found that the RL_{100y} for the North Sea is 10 – 20 cm higher than today by the 2080 year in the SRES A2 scenario (the standard high emissions scenario) considering only atmospheric-induced effects. Lowe et al., 2005 found that taking into account all the sea level components (i.e. the total relative sea level), the RL_{50y} at the eastern coast of Denmark becomes approximately 40 - 60 cm higher than today for the end of the 21th century in the B2 and A2 scenarios selected from the medium-high emissions scenarios family. In our case, the RL_{50y} is approximately 70 cm with 95%CI of [32-103] cm in the RCP 4.5 scenario (130 cm with 95%CI of [72-216] cm for the RCP 8.5) which is consistent with the results from Lowe et al., 2005.

Selected periods with extreme sea level events from the regional climate model simulations will be downscaled to the local level using the high resolution models by CAM and ICL.

It must be noted that this analysis is based on the results from one model with only one downscaled realization of each scenario. This fact does not allow us to assess the uncertainties of the projections for the sea level. Nevertheless, it is worth to mention that the model agrees well with the observations in the validation simulation and the trends of the sea level are consistent with similar the trends found by other authors. This gives us confidence in the reliability of the simulated climate projections. However, according with the IPCC AR5 the uncertainties of the total sea level changes are still considered *high*[1] mainly due to the uncertainties in the ice melting processes from ice sheets and glaciers (IPCC AR5). Concerning the uncertainties of atmospheric processes, although the poleward shift of the atmospheric circulation in the projected future climate is consistent among the GCMs in the IPCC AR5 simulations, the response of the storm track to such atmospheric circulation shift is substantially different in many GCMs. This suggests that the storm track projections for the North Atlantic and Europe which storm surges are based on still have a *low*[1] confidence (Christensen et al. 2013 – IPCC AR5 Chapter 14). In order to address the reduction of the uncertainties it would be desirable to perform an ensemble of simulations using different regional climate models forced by different global models.

[1] – Confidence level as defined at chapter 1 at the AR5 IPCC (Cubasch et al., 2013)

7 Acknowledgments

The authors acknowledge the input of Gabriel Jordá and Marta Marcos from the University of the Balearic Islands, Palma de Mallorca, Spain, for sharing their methodologies to analyse extreme sea level events.

8 References

ArcGIS (2010), Technical Reference and Documentation, Esri Software.Androulidakis, Y. S.; Kombiadou,

K. D.; Makris, C. V.; Baltikas, V. N. & Krestenitis, Y. N. Storm surges in the Mediterranean Sea: Variability and trends under future climatic conditions Dynamics of Atmospheres and Oceans, 2015, 71, 56-82

Bamber, J. and Riva, R.: The sea level fingerprint of recent ice mass fluxes, The Cryosphere, 4, 621-627, doi:10.5194/tc-4-621-2010, 2010.

Booij N., R.C. Ris and L.H. Holthuijsen (1999). A third-generation wave model for coastal regions, Part I - Model description and validation. Journal of Geophysical Research, 104, C4, 7649-7666.

Conte, D. & Lionello, P. Characteristics of large positive and negative surges in the Mediterranean Sea and their attenuation in future climate scenarios Global and Planetary Change, 2013, 111, 159-173

Cubasch, U., D. Wuebbles, D. Chen, M.C. Facchini, D. Frame, N. Mahowald, and J.-G. Winther, 2013: Introduction. In: Climate Change 2013: The Physical Science Basis. Contribution of Working Group I to the Fifth Assessment Report of the Intergovernmental Panel on Climate Change [Stocker, T.F., D. Qin, G.-K. Plattner, M. Tignor, S.K. Allen, J. Boschung, A. Nauels, Y. Xia, V. Bex and P.M. Midgley (eds.)]. Cambridge University Press, Cambridge, United Kingdom and New York, NY, USA.

Davies AM, Jones JE (1995) The influence of bottom and internal friction upon tidal currents: Taylor's problem in three dimensions. Cont Shelf Res 15(10):1251–1285. doi:10.1016/0278-4343(94)00076-Y

Elizalde, A., 2011: The water cycle in the Mediterranean region and the impacts of climate change. Max Planck Institute for Meteorology Rep. on Earth System Science 103, 128 pp.

Feistel, R.; Nausch, G.; W., M. & E., H. Temporal and spatial evolution of the Baltic deep water renewal in spring 2003 Oceanologia, 2003, 45(4), 623-642

Ford et al., A nonhydrostatic finite-element model for three-dimensional stratified oceanic flows. Part I: model formulation, Mon. Wea. Rev., 132, 2816-2831, 2004.

Geng QZ, Sugi M (2003) Possible change of extratropical cyclone activity due to enhanced green-house gases and sulfate aerosols—Study with a high-resolution AGCM. J Climate 16:2262–2274

Giorgetta, M. A., Jungclaus, J. H., Reick, C. H., Legutke, S., Bader, J., Böttinger, M., Brovkin, V., Crueger, T., Esch, M., Fieg, K., Glushak, K., Gayler, V., Haak, H., Hollweg, H.-D., Ilyina, T., Kinne, S., Kornblueh, L., Matei, D., Mauritsen, T., Mikolajewicz, U., Mueller, W. A., Notz, D., Pithan, F., Raddatz, T., Rast, S., Redler, R., Roeckner, E., Schmidt, H., Schnur, R., Segschneider, J., Six, K., Stockhause, M., Timmreck, C., Wegner, J., Widmann, H., Wieners, K.-H., Claussen, M., Marotzke, J., & Stevens, B. (2013). Climate and carbon cycle changes from 1850 to 2100 in MPI-ESM simulations for the coupled model intercomparison project phase 5. Journal of Advances in Modeling Earth Systems, 5, 572-597.

Giuseppe Zappa, Len C. Shaffrey, Kevin I. Hodges, Phil G. Sansom, and David B. Stephenson, 2013: A Multimodel Assessment of Future Projections of North Atlantic and European Extratropical Cyclones in the CMIP5 Climate Models*. J. Climate, 26, 5846–5862.
doi: http://dx.doi.org/10.1175/JCLI-D-12-00573.1

Gräwe, U.; Burchard, H.; Müller, M. & Schuttelaars, H. M. Seasonal variability in M2 and M4 tidal constituents and its implications for the coastal residual sediment transport Geophys. Res. Lett., 2014, 41, 5563-5570

Hagemann, S. & Dümenil, L. A parametrization of the lateral waterflow for the global scale Climate Dynamics, 1998, 14, 17-31

Hallegatte S., Patmore N., Mestre O., Dumas P., Corfee-Morlot Jan., Herweijer C. and Muir-Wood R.. (2008), "Assessing Climate Change Impacts, Sea Level Rise and Storm Surge Risk in Port Cities: A Case Study on Copenhagen", OECD Environment Working Papers, No. 3, OECD Publishing. http://dx.doi.org/10.1787/236018165623

He, Y.(2011).Initial tests of suitability of 3D modelling in urban flooding.(Master's thesis, Imperial College London, London, United Kingdom).

IOC, 2012 Global Sea Level Observing System (GLOSS) Implementation Plan – 2012. UNESCO/IOC, 41pp. 2012. (IOC Technical Series No.100)

IPCC AR5 - Church, J.A., P.U. Clark, A. Cazenave, J.M. Gregory, S. Jevrejeva, A. Levermann, M.A. Merrifield, G.A. Milne, R.S. Nerem, P.D. Nunn, A.J. Payne, W.T. Pfeffer, D. Stammer and A.S. Unnikrishnan, 2013: Sea Level Change. In: Climate Change 2013: The Physical Science Basis. Contribution of Working Group I to the Fifth Assessment Report of the Intergovernmental Panel on Climate Change [Stocker, T.F., D. Qin, G.-K. Plattner, M. Tignor, S.K. Allen, J. Boschung, A. Nauels, Y. Xia, V. Bex and P.M. Midgley (eds.)]. Cambridge University Press, Cambridge, United Kingdom and New York, NY, USA. 2013.

Jacob, D. A note to the simulation of the annual and inter-annual variability of the water budget over the Baltic Sea drainage basin. Meteorol. Atmos. Phys. 2001, 77, 61

Jacob, D.; Petersen, J.; Eggert, B.; Alias, A.; Christensen, O. B.; Bouwer, L.; Braun, A.; Colette, A.; Déqué, M.; Georgievski, G.; Georgopoulou, E.; Gobiet, A.; Menut, L.; Nikulin, G.; Haensler, A.; Hempelmann, N.; Jones, C.; Keuler, K.; Kovats, S.; Kröner, N.; Kotlarski, S.; Kriegsmann, A.; Martin, E.; Meijgaard, E.; Moseley, C.; Pfeifer, S.; Preuschmann, S.; Radermacher, C.; Radtke, K.; Rechid, D.; Rounsevell, M.; Samuelsson, P.; Somot, S.; Soussana, J.-F.; Teichmann, C.; Valentini, R.; Vautard, R.; Weber, B. & Yiou, P. EURO-CORDEX: new high-resolution climate change projections for European impact research Regional Environmental Change, Springer Berlin Heidelberg, 2013, 1-16

Jordà, G.; Gomis, D.; Álvarez-Fanjul, E. & Somot, S. Atmospheric contribution to Mediterranean and nearby Atlantic sea level variability under different climate change scenarios Global and Planetary Change, 2012, 80-81, 198-214

Limerinos, J. T. (1970). Determination of the Manning coefficient from measured bed roughness in natural channels.

Lowe, J. & Gregory, J. The effects of climate change on storm surges around the United Kingdom Philosophical Transactions of the Royal Society of London A: Mathematical, Physical and Engineering Sciences, 2005, 363, 1313-1328

Marcos, M.; Tsimplis, M. N. & Shaw, A. G. P. Sea level extremes in southern Europe J. Geophys. Res., 2009, 114.

Marzeion, B., Jarosch, A. H., and Hofer, M.: Past and future sea-level change from the surface mass balance of glaciers, The Cryosphere, 6, 1295-1322, doi:10.5194/tc-6-1295-2012, 2012.

Mikolajewicz, U.; Sein, D.; Jacob, D.; Königk, T.; Podzun, R. & Semmler, T. Simulating Arctic sea ice variability with a coupled regional atmosphere-ocean-sea ice model Meteorologische Zeitschrift, 2005, 14, No.6, 793-800

Mudersbach, C. & Jensen, J. Nonstationary extreme value analysis of annual maximum water levels for designing coastal structures on the German North Sea coastline Journal of Flood Risk Management, Blackwell Publishing Ltd, 2010, 3, 52-62

Oberhuber, J.M., Herzog, M., Graf, H.-F., and Schwanke, K., Volcanic Plume Simulation on Large Scales, J. Volcanol. Geotherm. Res., 87, 29-53, 1998.

Pawlowicz, R., B. Beardsley, and S. Lentz, "Classical Tidal Harmonic Analysis Including Error Estimates in MATLAB using T_TIDE", Computers and Geosciences, 28, 929-937 (2002).

Riahi, K., V. Krey, S. Rao, V. Chirkov, G. Fischer, P. Kolp, G. Kindermann, N. Nakicenovic, and P. Rafai (2011), RCP-8.5: Exploring the consequence of high emission trajectories, Clim. Change, 109, 33–57, doi:10.1007/s10584-011-0149-y.

Roos, P.; Velema, J.; Hulscher, S. & Stolk, A. An idealized model of tidal dynamics in the North Sea: resonance properties and response to large-scale changes Ocean Dynamics, Springer-Verlag, 2011, 61, 2019-2035

Savcenko R., Bosch W., Dettmering D., Seitz F.: EOT11a - Global Empirical Ocean Tide model from multi-mission satellite altimetry, with links to model results. Deutsches Geodätisches Forschungsinstitut, Munich, 10.1594/PANGAEA.834232, 2012

Seifert T., Tauber F. and Kayser B. (2001). A high resolution spherical grid topography of the Baltic Sea – 2nd edition, Baltic Sea Science Congress, Stockholm 25-29. November 2001, Poster #147, www.io-warnemuende.de/iowtopo

Sein, D. V., Mikolajewicz, U., Gröger, M., Fast, I., Cabos, W., Pinto, J. G. & Jacob, D. (2015). Regionally coupled atmosphere-ocean-sea ice-marine biogeochemistry model ROM: 1. Description and validation. Journal of Advances in Modeling Earth Systems, 7(1), 268-304.

Sinha B, Pingree RD (1997) The principal lunar semidiurnal tide and its harmonics: baseline solutions for M2 and M4 constituents in the North-West European Continental Shelf. Cont Shelf Res 17(11):1321–1365. doi:10.1016/S0278-4343(97)00007-1

Stocker, T.F., D. Qin, G.-K. Plattner, L.V. Alexander, S.K. Allen, N.L. Bindoff, F.-M. Bréon, J.A. Church, U. Cubasch, S. Emori, P. Forster, P. Friedlingstein, N. Gillett, J.M. Gregory, D.L. Hartmann, E. Jansen, B. Kirtman, R. Knutti, K. Krishna Kumar, P. Lemke, J. Marotzke, V. Masson-Delmotte, G.A. Meehl, I.I. Mokhov, S. Piao, V. Ramaswamy, D. Randall, M. Rhein, M. Rojas, C. Sabine, D. Shindell, L.D. Talley, D.G. Vaughan and S.-P. Xie, 2013: Technical Summary. In:

Climate Change 2013: The Physical Science Basis. Contribution of Working Group I to the Fifth Assessment Report of the Intergovernmental Panel on Climate Change [Stocker, T.F., D. Qin, G.-

Soledad, B. R.(2014). Modelling flooding from the sea interacting with the drainage system under the influence of combined flood hazards to develop risk management strategies for the coastal region of Greve, Denmark. (Master's thesis, University of Nice Sophia Antipolis, Nice, France).

K. Plattner, M. Tignor, S.K. Allen, J. Boschung, A. Nauels, Y. Xia, V. Bex and P.M. Midgley (eds.)]. Cambridge University Press, Cambridge, United Kingdom and New York, NY, USA.

Suendermann, J. & Pohlmann, T. A brief analysis of North Sea physics Oceanologia, 2011, 53, 663-689

Thomas, M., Sündermann, J., and Maier-Reimer, E.: Consideration of ocean tides in an OGCM and impacts on subseasonal to decadal polar motion excitation, Geophys. Res. Lett., 28, 2457–2460, 2001.

Thomson, A. M., et al. (2011), RCP4.5: A pathway for stabilization of radiative forcing by 2100, Clim. Change, 109, 77–94, doi:10.1007/s10584-011-0151-4.

Uppala, S.; Kallberg, P.; Simmons, A.; Andrae, U.; da Costa Bechtold, V.; Fiorino, M.; Gibson, J.; Haseler, J.; Hernandez, A.; Kelly, G.; Li, X.; Onogi, K.; Saarinen, S.; Sokka, N.; Allan, R.; Andersson, E.; Arpe, K.; Balmaseda, M.; Beljaars, A.; van de Berg, L.; Bidlot, J.; Bormann, N.; Caires, S.; Chevallier, F.; Dethof, A.; Dragosavac, M.; Fisher, M.; Fuentes, M.; Hagemann, S.; Holm, E.; Hoskins, B.; Isaksen, L.; Janssen, P.; Jenne, R.; McNally, A.; Mahfouf, J.-F.; Morcrette, J.-J.; Rayner, N.; Saunders, R.; Simon, P.; Sterl, A.; Trenberth, K.; Untch, A.; Vasiljevic, D.; Viterbo, P. & Woollen, J. The ERA-40 re-analysis Quart. J. Roy. Meteor. Soc., 2005, 131, 2961-3012

Vizcaíno, M., Mikolajewicz, U., Ziemen, F., Rodehacke, C., Greve, R., & van den Broeke, M. (2015). Coupled simulations of the Greenland ice sheet and climate change up to AD 2300. Geophysical Research Letters, 42, 3927–3935.

Wakelin, S. L.; Woodworth, P. L.; Flather, R. A. & Williams, J. A. Sea-level dependence on the NAO over the NW European Continental Shelf Geophys. Res. Lett., 2003, 30.

Woth, K.; Weisse, R. & von Storch, H. Climate change and North Sea storm surge extremes: an ensemble study of storm surge extremes expected in a changed climate projected by four different regional climate models Ocean Dynamics, Ocean Dynamics, Springer-Verlag, 2005, 56, 3-15.

J. Zheng, J. Zhu , Z. Wang , F. Fang , C. C. Pain , and J. Xiang, Towards a new multiscale air quality transport model using the fully unstructured anisotropic adaptive mesh technology of Fluidity (version 4.1.9) Geosci. Model Dev., 8, 3421-3440, 2015.

pearl
Preparing for Extreme And Rare events in coastal regions